Theor Chem Acc (2011) 130:991–1000
DOI 10.1007/s00214-011-1038-1

REGULAR ARTICLE

Effect of non-specificity in shape, size, and dielectric properties on electromagnetic extinction and optical field enhancement from spherical nanolayered metal-dielectric particles

Anil K. Kodali · Rohit Bhargava

Received: 1 August 2011 / Accepted: 3 September 2011 / Published online: 18 October 2011

Abstract Metal-dielectric composite nanospheres can amplify the scattering, emission, and absorption signature of molecules in their vicinity. Their ability to redistribute electromagnetic fields and produce pockets of greatly amplified fields is the dominant cause in achieving enhancement effects, for example, for surface-enhanced Raman spectroscopy. Extensive use of the field amplification has been made in devising ultrasensitive tag (label)–based spectroscopic techniques. For example, we have recently proposed nano-layered alternating metal-dielectric particles (nano-LAMP)—a symmetric implementation of which is a nanoparticle consisting of alternating metal and dielectric shells. Exceptional spatial and spectral control on amplification can be achieved by designing the size and location of metal and dielectric layers in this geometry. Theoretical understanding exists and an engineering optimization approach can be adapted to design a palette of probes exploiting this control and tunability. However, current fabrication techniques are limited in their ability to achieve the required specificity in the spherical configurations. Hence, we investigate here the effects of variability, introduced by fabrication approaches into the structure of nano-LAMPs, on their spectroscopic signature. In particular, theoretical results are presented for the effects on enhancement due to variability in size, shape, and dielectric environment in the cases of gold–silica, silver–silica, and copper–silica nano-LAMPs. The results obtained show that the shape and dielectric properties of the metal shell play a crucial role in experimentally realizing the specificity of the magnitude of the enhancement and determine the key parameters to control and test in experimental validations.

Keywords Spectroscopic enhancement · Nanoparticles · Electromagnetic scattering · Mie theory

Dedicated to Professor Akira Imamura on the occasion of his 77th birthday and published as part of the Imamura Festschrift Issue.

A. K. Kodali · R. Bhargava (✉)
Department of Mechanical Science and Engineering, University of Illinois at Urbana-Champaign, 4265 Beckman Institute, 405 North Mathews Avenue, Urbana, IL 61801, USA
e-mail: rxb@illinois.edu
URL: http://chemimage.illinois.edu

A. K. Kodali · R. Bhargava
Micro and Nanotechnology Laboratory, University of Illinois at Urbana-Champaign, 4265 Beckman Institute, 405 North Mathews Avenue, Urbana, IL 61801, USA

A. K. Kodali · R. Bhargava
Beckman Institute of Advanced Science and Technology, University of Illinois at Urbana-Champaign, 4265 Beckman Institute, 405 North Mathews Avenue, Urbana, IL 61801, USA

R. Bhargava
Departments of Bioengineering and Electrical and Computer Engineering, The University of Illinois Cancer Center, University of Illinois at Urbana-Champaign, 4265 Beckman Institute, 405 North Mathews Avenue, Urbana, IL 61801, USA

1 Introduction

Metal nanoparticles are known to exhibit distinct optical and colorimetric characteristics compared to the corresponding bulk metal [1]. The nanoscale properties [2] are attributed to surface plasmons [3]—collective oscillations of electrons at the surface when irradiated. When the nanoparticle is illuminated, the surface electrons can both absorb incident electromagnetic energy or scatter it resulting in a net extinction of the incident energy [4]. The extent to which a particular optical frequency is attenuated is dependent on the size, shape, and dielectric property of

the metal nanoparticle/surface [5], and optical resonances can be achieved via surface plasmons [6, 7]. The scattering and absorption of energy also leads to a spatial redistribution of electromagnetic fields in the nanoparticle's vicinity, often resulting in regions of amplified electromagnetic fields (hot spots) [8]. Gold, silver, and copper nanospheres in the size ranges ~5–200 nm, for example, possess such size-based controllability in the optical signature and ability to generate hot spots under visible and near-IR illuminations [9, 10]. Hence, these nanoparticles have been extensively used in optical spectroscopic sensing applications: both as tags/labels [11] for molecules and as contrast agents [12] to enhance the emission/absorption characteristics of molecules in their vicinity (hot spots). Monolithic metal nanospheres, however, have relatively wider resonances and lower enhancement characteristics. Hence, many groups have attempted to design and use composite nanoparticles that are structured at the nanometer length scales [11, 13–22].

Structured nanoparticles, in particular layered nanospheres, can possess narrower resonances and greatly increase the optical tunability as well as amplification characteristics when compared to a monolithic metal nanoparticle of the same size [23]. Hence, structured particles have found increasing popularity recently due to the optical response advantages combined with the advances in theoretical understanding [14, 15, 24–27] and fabrication [18, 19, 21, 22, 28, 29] making them tractable for use. We have recently proposed a design template based on layered nanospheres with alternating metal and dye-embedded silica layers to achieve optical labels (shown in Fig. 1), titled nano-layered alternating metal-dielectric particle (nano-LAMP) [17, 20]. As opposed to nanoshells [28] or other geometries like COINs [22] and nanocrescents [19], this configuration provides a larger parameter space that enables optimization and fine control over the optical response of particles. Certainly, the geometry provides both a computational and fabrication challenge in navigating the design and fabrication parameters to design particles for specific use. Excellent theoretical understanding [26] for modeling their optical responses based on layered-Mie [30] theory-based solutions exists. Using the nano-LAMP template, we have demonstrated theoretically an engineering approach toward designing a palette of Raman and optical labels with designed sensitivity and selectivity. The predicted performance includes particles for ultrasensitive analysis, for example, specific nano-LAMP designs are predicted to obtain up to 12 orders of magnitude signal higher than that from a single molecular of analyte to which they may bind [20]. Such designs, however, comprise extremely thin metal and silica shells stretching the limits of fabrication. Further, the precision of such fabrication is difficult, providing a large confounding aspect to the ultimate practical use of the nano-LAMP designs. As a consequence, it is important to study both the theoretical predictions of ideal and distorted structures as well as make advances in fabrication processes that exist for simple nanostructures but need to be better tuned or optimized to make controlled nanolayers multiple times.

With currently available fabrication techniques [31], for example, each concentric shell in the nano-LAMP can be achieved in two steps [32, 33]. The first step involves establishing a layer of seeds of nanoparticles (metal or dye-embedded silica) attached to the previous layer or core using molecular linkers. The second step is to grow this layer into a continuous shell by reducing metal onto it in case of metal shells and fusing silica in case of silica layer [34]. Established techniques [35] exist for each step in this process, but considerable variability is induced into the final structure from each step. For example, the variability in sizes of nanoparticle seeds can result in a slight variation in the final shape of structure. Also, the variability in fusing silica or reducing metal shells can result in a slight variation in the sizes of the layers. Hence, the first aspect to investigate is whether small variations in size and shape can affect the overall optical properties of the nano-LAMPs to an appreciable extent. An understanding of the dependence of optical response on size and shape will help estimate the practicality of use of these structures as well as provide guidelines for the precision required in fabrication. While estimating size irregularities is possible either in design or in electron microscopy measurements of the fabricated structures, care must also be taken to account for the sharp change in material properties with size at this length scale. The standard refractive index profiles available for bulk metal [36, 37] are not applicable for thin metal shells that are comparable in size to the mean free path of conduction for electrons [38]. Similarly, fabrication can introduce small voids [39] within the layer that result in

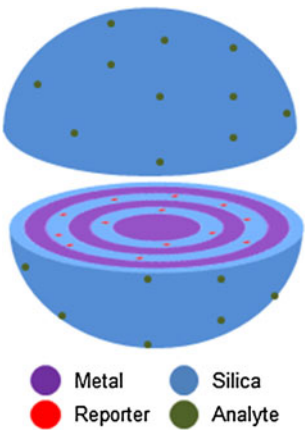

Fig. 1 Nanolayered alternating metal-dielectric probe (nano-LAMP) sliced in the *middle* to show structure

a change in the dielectric properties of metal and silica. Here, we theoretically investigate the effect of small variations in size, shape, and dielectric properties for nano-LAMPs. The primary goal is to employ the predictions to understand the stability (and variation) of optical responses of nano-LAMPs with changes in different geometric and material parameters.

2 Theory, implementation, and computational details

A detailed description of theoretical modeling of optical responses of nano-LAMPs has been discussed elsewhere [14, 20]. For providing a better understanding of the formulation in the context of results presented, here, we provide the details of theoretical approach again. Although the actual response of dye molecules within the dielectric shells can also be influenced by enhancement due to chemical charge transfer effects [40, 41], we ignore it and focus on the much dominant electromagnetic effects [42]. The uniform distribution of dyes within the silica shells, which minimizes the surface-active sites and chemical enhancement effects [43], also justifies this approach. We thus base our solution purely on electromagnetic scattering by these particles. A layered-Mie [30] theory-based formulation has been developed to obtain analytical solutions for scattering and absorption characteristics of nano-LAMPs. Since the particles considered here are much smaller than the incident wavelength of excitation, it suffices to consider a single plane wave excitation instead of a focused incident beam [44].

Let us consider the case of an N layered sphere with each jth layer having a relative refractive index m_j with respect to the refractive index of the surrounding medium. Since we are interested in electric fields, we can consider the sphere and surrounding medium to have a magnetic permeability of 1. An incident wave propagating along positive z-axis and polarized along positive x-axis can be used without any loss of generality owing to the spherical symmetry of the problem. This field is:

$$\vec{\mathbf{E}}_{\text{inc}} = E_0 e^{i\kappa z}\hat{e}_x, \tag{1}$$

with κ being the propagation constant in the embedding medium.

The incident plane wave field can be expanded in terms of geometrically similar basis functions (vector spherical harmonics, VSH—**M** and **N**) to the spherical interfaces between the layers, as:

$$\begin{aligned}\vec{\mathbf{E}}_{\text{inc}} &= E_0\sum_{n=1}^{\infty} i^n \frac{2n+1}{n(n+1)}\left(\vec{\mathbf{M}}^{(1)}_{o1n} - i\vec{\mathbf{N}}^{(1)}_{e1n}\right)\\ \vec{\mathbf{H}}_{\text{inc}} &= -\frac{\kappa}{\omega}E_0\sum_{n=1}^{\infty} i^n \frac{2n+1}{n(n+1)}\left(\vec{\mathbf{M}}^{(1)}_{e1n} + i\vec{\mathbf{N}}^{(1)}_{o1n}\right)\end{aligned} \tag{2}$$

Similar expansions for the scattered field are:

$$\begin{aligned}\vec{\mathbf{E}}_{\text{sc}} &= E_0\sum_{n=1}^{\infty} i^n \frac{2n+1}{n(n+1)}\left(a_n^{(N+1)}\vec{\mathbf{M}}^{(3)}_{o1n} - ib_n^{(N+1)}\vec{\mathbf{N}}^{(3)}_{e1n}\right)\\ \vec{\mathbf{H}}_{\text{sc}} &= -\frac{\kappa}{\omega}E_0\sum_{n=1}^{\infty} i^n \frac{2n+1}{n(n+1)}\left(b_n^{(N+1)}\vec{\mathbf{M}}^{(3)}_{e1n} + ia_n^{(N+1)}\vec{\mathbf{N}}^{(3)}_{o1n}\right)\end{aligned} \tag{3}$$

The fields in jth layer within the sphere are:

$$\begin{aligned}\vec{\mathbf{E}}_j &= E_0\sum_{n=1}^{\infty} i^n \frac{2n+1}{n(n+1)}\\ &\quad\times\left(A_n^j\vec{\mathbf{M}}^{(1)}_{o1n} - iB_n^j\vec{\mathbf{N}}^{(1)}_{e1n} + C_n^j\vec{\mathbf{M}}^{(3)}_{o1n} - iF_n^j\vec{\mathbf{N}}^{(3)}_{e1n}\right)\\ \vec{\mathbf{H}}_j &= -\frac{\kappa_j}{\omega}E_0\sum_{n=1}^{\infty} i^n \frac{2n+1}{n(n+1)}\\ &\quad\times\left(B_n^j\vec{\mathbf{M}}^{(1)}_{e1n} + iA_n^j\vec{\mathbf{N}}^{(1)}_{o1n} + F_n^j\vec{\mathbf{M}}^{(3)}_{e1n} + iC_n^j\vec{\mathbf{N}}^{(3)}_{o1n}\right)\end{aligned} \tag{4}$$

The superscripts 1 and 3 on VSH (**M** and **N**) are dependent on using spherical Bessel (inward waves) or Hankel functions (outward waves), respectively. The fields are expanded in appropriate VSH (Bessel or Hankel) based on the requirements of being mathematically well defined (the incident field has to be well defined and be zero at the origin, and the scattered field has to be finite at infinity). The internal fields on the other hand can be a combination of both inward and outward waves, and accordingly, both the Bessel functions of first kind and Hankel functions are chosen to define them. The propagation constant in jth layer appearing in Eq. 4 is given by $\kappa_j = 2\pi m_j/\lambda$. The analytical expressions for VSH are given by:

$$\begin{aligned}&\mathbf{M}_{o1n}(\kappa r,\theta,\phi)\\ &\quad= z_n(\kappa r)\pi_n(\cos\theta)\cos\phi\,\hat{e}_\theta - z_n(\kappa r)\tau_n(\cos\theta)\sin\phi\,\hat{e}_\phi,\\ &\mathbf{M}_{e1n}(\kappa r,\theta,\phi)\\ &\quad= -z_n(\kappa r)\pi_n(\cos\theta)\sin\phi\,\hat{e}_\theta - z_n(\kappa r)\tau_n(\cos\theta)\cos\phi\,\hat{e}_\phi,\\ &\mathbf{N}_{o1n}(\kappa r,\theta,\phi)\\ &\quad= n(n+1)\frac{z_n(\kappa r)}{\kappa r}\pi_n(\cos\theta)\sin\phi\,\hat{e}_r\\ &\qquad+\frac{\mathrm{d}(\kappa r z_n(\kappa r))}{\mathrm{d}(\kappa r)}\left[\tau_n(\cos\theta)\sin\phi\,\hat{e}_\theta + \pi_n(\cos\theta)\cos\phi\,\hat{e}_\phi\right],\\ &\mathbf{N}_{e1n}(\kappa r,\theta,\phi) = n(n+1)\frac{z_n(\kappa r)}{\kappa r}\pi_n(\cos\theta)\cos\phi\,\hat{e}_r\\ &\qquad+\frac{\mathrm{d}(\kappa r z_n(\kappa r))}{\mathrm{d}(\kappa r)}\left[\tau_n(\cos\theta)\cos\phi\,\hat{e}_\theta - \pi_n(\cos\theta)\sin\phi\,\hat{e}_\phi\right],\end{aligned} \tag{5}$$

where z_n are appropriate first-order Bessel functions (j_n) or Hankel functions ($h_n^{(1)}$). The angle-dependent functions are

functions of associated Legendre polynomials and are given as:

$$\pi_n = \frac{P_n^{(1)}(\cos\theta)}{\sin\theta}, \quad \tau_n = \frac{\mathrm{d}P_n^{(1)}(\cos\theta)}{\mathrm{d}\theta} \tag{6}$$

We need to evaluate the coefficients of expansion, A_n, B_n, C_n, F_n, $a_n^{(N+1)}$, and $b_n^{(N+1)}$ in Eqs. 1–4. These can be obtained by enforcing the continuity conditions at the interfaces. To accommodate the discontinuity between jth and $(j+1)$th layer, we have:

$$\begin{aligned}(\mathbf{E}_{j+1} - \mathbf{E}_j) \times \hat{e}_r = 0 \\ (\mathbf{H}_{j+1} - \mathbf{H}_j) \times \hat{e}_r = 0\end{aligned} \tag{7}$$

Similarly, the boundary conditions between the outermost layer and surrounding medium would lead to:

$$\begin{aligned}(\mathbf{E}_{sc} + \mathbf{E}_{inc} - \mathbf{E}_N) \times \hat{e}_r = 0 \\ (\mathbf{H}_{sc} + \mathbf{H}_{inc} - \mathbf{H}_N) \times \hat{e}_r = 0\end{aligned} \tag{8}$$

Ricatti-Bessel functions (defined as $\psi_n(\rho) = \rho j_n(\rho)$, $\xi(\rho) = \rho h_n^{(1)}(\rho)$), logarithmic derivative functions ($D_n^{(1)}(\rho) = \psi_n'(\rho)/\psi_n(\rho)$, $\mathrm{D}_n^{(3)}(\rho) = \xi_n'(\rho)/\xi_n(\rho)$), and ratio functions ($R_n(\rho) = \psi_n(\rho)/\xi_n(\rho)$) can be used to reformulate the above equations in order to obtain stable recursive formulations. To further simplify and stabilize the formulation, we define: $a_n^j = \frac{C_n^j}{A_n^j}$, $b_n^j = \frac{F_n^j}{B_n^j}$. In this formulation, we start with core, where $a_n^1 = b_n^1 = 0$, and evaluate the rest of the coefficients a_n^j and b_n^j from the values a_n^{j-1} and b_n^{j-1}. Defining x as the size parameter given by $x = 2\pi r/\lambda$, for $j = 2,\ldots,N$, we have the following equations.

$$\begin{aligned}&U_n(m_{j-1}x_{j-1}) \\ &= m_{j-1}\frac{R_n(m_{j-1}x_{j-1})D_n^{(1)}(m_{j-1}x_{j-1}) + a_n^{j-1}D_n^{(3)}(m_{j-1}x_{j-1})}{R_n(m_{j-1}x_{j-1}) + a_n^{j-1}}, \\ &V_n(m_{j-1}x_{j-1}) \\ &= \frac{1}{m_{j-1}}\frac{R_n(m_{j-1}x_{j-1})D_n^{(1)}(m_{j-1}x_{j-1}) + b_n^{j-1}D_n^{(3)}(m_{j-1}x_{j-1})}{R_n(m_{j-1}x_{j-1}) + b_n^{j-1}}, \\ &a_n^j = -R_n(m_jx_{j-1})\frac{U_n(m_{j-1}x_{j-1}) - m_jD_n^{(1)}(m_jx_{j-1})}{U_n(m_{j-1}x_{j-1}) - m_jD_n^{(3)}(m_jx_{j-1})}, \\ &b_n^j = -R_n(m_jx_{j-1})\frac{m_jV_n(m_{j-1}x_{j-1}) - D_n^{(1)}(m_jx_{j-1})}{m_jV_n(m_{j-1}x_{j-1}) - D_n^{(3)}(m_jx_{j-1})}.\end{aligned} \tag{9}$$

The coefficients of the scattered field can be obtained as:

$$\begin{aligned}a_n^{N+1} &= -R_n(x_N)\frac{U_n(m_Nx_N) - D_n^{(1)}(x_N)}{U_n(m_Nx_N) - D_n^{(3)}(x_N)}, \\ b_n^{N+1} &= -R_n(x_N)\frac{V_n(m_Nx_N) - D_n^{(1)}(x_N)}{V_n(m_Nx_N) - D_n^{(3)}(x_N)}.\end{aligned} \tag{10}$$

From this point, the remaining internal coefficients can be obtained by starting at the outer layer and using inward recursion. For the outer layer we have:

$$\begin{aligned}A_n^N &= m_N\frac{\xi_n(x_N)}{\xi_n(m_Nx_N)}\left(\frac{R_n(x_N) + a_n^{N+1}}{R_n(m_Nx_N) + a_n^N}\right), \\ B_n^N &= \frac{\xi_n(x_N)}{\xi_n(m_Nx_N)}\left(\frac{R_n(x_N) + b_n^{N+1}}{R_n(m_Nx_N) + b_n^N}\right).\end{aligned} \tag{11}$$

For the inner layers $j = N,\ldots,2$ we have:

$$\begin{aligned}A_n^{j-1} &= A_n^j\frac{m_{j-1}}{m_j}\frac{\xi_n(m_jx_{j-1})}{\xi_n(m_{j-1}x_{j-1})}\left(\frac{R_n(m_jx_{j-1}) + a_n^j}{R_n(m_{j-1}x_{j-1}) + a_n^{j-1}}\right), \\ B_n^{j-1} &= B_n^j\frac{\xi_n(m_jx_{j-1})}{\xi_n(m_{j-1}x_{j-1})}\left(\frac{R_n(m_jx_{j-1}) + b_n^j}{R_n(m_{j-1}x_{j-1}) + b_n^{j-1}}\right).\end{aligned} \tag{12}$$

Using appropriate cutoff for the maximum order of VSH and these analytical functions [45], and stable recursive evaluation of the logarithmic derivative and ratio functions involved, an accurate mathematical solution for the EM fields can be obtained. The far-fields are dependent on the coefficients of scattered field and can be evaluated using the asymptotic expansions of the scattered fields. The scattering and extinction efficiencies in the far-field are obtained using:

$$\begin{aligned}Q_{\mathrm{ext}} &= \frac{2}{\kappa r_t^2}Re\left\{\sum_{n=1}^{\infty}(2n+1)\left(a_n^{(N+1)} + b_n^{(N+1)}\right)\right\}, \\ Q_{\mathrm{sca}} &= \frac{2}{\kappa r_t^2}\left\{\sum_{n=1}^{\infty}(2n+1)\left(\left|a_n^{(N+1)}\right|^2 + \left|b_n^{(N+1)}\right|^2\right)\right\},\end{aligned} \tag{13}$$

where r_t is the total size of the particle. For metal layers of thickness greater than 5 nm, it is typically acceptable to use the bulk values. In case of metal shells thinner than 5 nm, a size-based correction [38] is implemented to account for the intrinsic size effects due to reduced mean free path of electrons.

3 Results and discussion

The interaction between surface plasmons associated with different metal shells in LAMPs determines their optical properties. The coupling of dipolar resonances results in stronger long-wavelength resonances while the higher-order multipole coupling results in short-wavelength resonances. The contributions and interplasmonic coupling from different shells also leads to a local reorganization of electric field within and in the vicinity of LAMPs. The internal electromagnetic distributions contribute to the overall enhancement of dye molecules embedded and

signal from the nano-LAMP. A convenient measure of enhancement in signal is the signal delivered by the LAMP compared to what would have been recorded directly from the analyte molecule that is tagged by the LAMP. The relative strength of interaction and manifestation of resonances is dependent on the overall size of the particle, relative thickness of the layers, and composition (refractive indices) of individual layers. Even a slight variation in these parameters could significantly affect the overall response of the particle recorded by far-field optical configurations and can cause a deviation from the predicted values by changing local field distributions. Here, we examine the variability using both far-field characteristics and internal electromagnetic distributions.

3.1 Variation in dielectric properties

The optical responses of metal nanoparticles are strongly dependent on the refractive indices of the chosen materials. The real part of the refractive index determines the energy scattered, while the imaginary part determines the energy absorbed. For nano-LAMPs, the energy reaching each shell is dependent on the attenuation of the outer shells. The overall scattering and absorption is thus a cumulative superposition of the scattering and absorption due to individual shells. The refractive index values for any metal layer, thus, play a crucial role, and any variability can affect both far-field and near-field characteristics. In the literature, the refractive index profiles of gold, copper, and silver are usually taken from two sources, Johnson et al. [36] and Palik et al [37]. These profiles determined from experiment differ to a small extent in some of the wavelength regions. To demonstrate the effect of refractive index variability, we consider the differences in optical characteristics of a nano-LAMP calculated using the two profiles. In all cases for this section, we use LAMPs with silica shells of dielectric constant 2.04 and consider that they are embedded in water-like media with dielectric constant 1.77 [25]. Figure 2 shows the influence of slight change in refractive index on extinction efficiencies of a 50 nm-sized 4-layered and 6-layered gold–silica LAMP. The differences in refractive indices obtained from smooth interpolation from experimental values given in the two sources are shown in Fig. 2a, b. The real parts differ slightly, primarily in the ~200–500 nm spectral region; the imaginary parts differ slightly as well, primarily in the ~600–1,000 nm region. The extinction of 4-layered and 6-layered LAMPs has two dominant resonance peaks, one at long wavelength due to coupling of dipolar resonances and one at shorter wavelength due to coupling of higher-order multipole resonances. The location of both dipolar and higher-order multipole resonances shifts slightly toward longer wavelengths when using data sets from

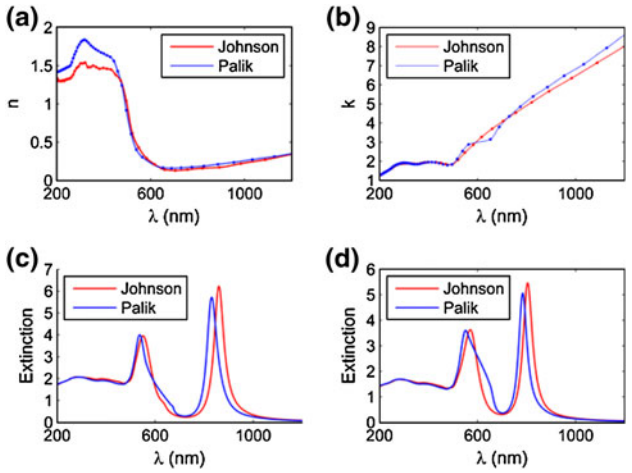

Fig. 2 Extinction efficiencies of gold–silica nano-LAMPs influenced by source chosen for refractive index profiles. Dispersion profiles for real (**a**) and imaginary parts (**b**) of refractive index. Extinction efficiencies using these profiles for 4-layered gold–silica LAMP (**c**) with radii: {26, 34, 44, 50 nm} and 6-layered gold–silica LAMP (**d**) with radii: {5, 12, 22, 31, 41, 50 nm}

Johnson et al. [36]. The shift to longer wavelength resonance is greater and significant, about 30 nm in case of 4-layered structures and about 20 nm in case of 6-layered structures. The cumulative contribution of different gold layers not only increases the signal but also amplifies the dependence of extinction on refractive index value chosen. Also, it can be noticed that absorption plays a dominant role in these profiles and shifts in resonances are consistent with shifts in the absorption index values. Given that these values are largely used by the academic community in calculating materials' responses, it may be fair to estimate that the fabrication uncertainty is of the same order. Though the resonance peaks are different, the feature itself is broad enough that substantial enhancement may be obtained with narrowband excitation lasers within the peak resonance. Thus, these materials and structures can potentially lead to effective use of particles, albeit the uncertainty in designing structures may be significant.

In the visible and NIR spectral regions, broadband illumination is often chosen for analysis, and nanoparticles are required to have a distinct pattern of narrow lines for these applications. Silver–silica LAMPs can be designed to have stronger and narrower resonances than other metals. With structures that possess such stronger inter-plasmonic coupling between the metal shells, the changes in extinction profiles with any slight changes in refractive index are also more obvious. For example, Fig. 3 shows extinction efficiencies of 4-layered (Fig. 3c) and 6-layered (Fig. 3d) silver–silica LAMPs along with the dispersion profiles of refractive index (Fig. 3a, b) presented in both sources. The real and imaginary parts of refractive index differ considerably in the wavelength ~300–1,200 nm. The extinction

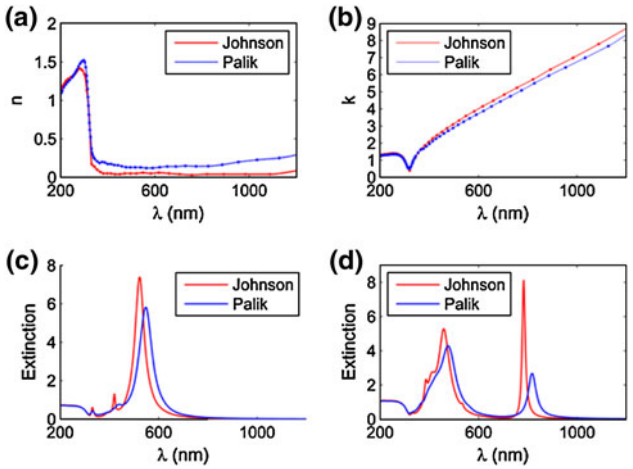

Fig. 3 Extinction efficiencies of silver–silica nano-LAMPs influenced by source chosen for refractive index profiles. Dispersion profiles for real (**a**) and imaginary parts (**b**) of refractive index. Extinction efficiencies using these profiles for 4-layered LAMP (**c**) with radii: {5, 22, 32, 50 nm} and 6-layered LAMP (**d**) with radii: {5, 10, 20, 25, 35, 50 nm}

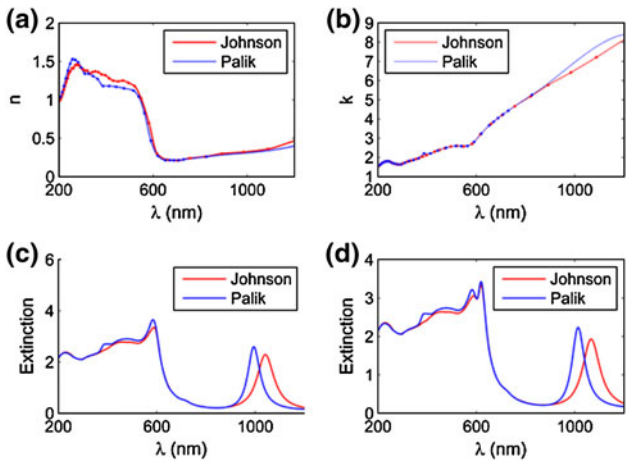

Fig. 4 Extinction efficiencies of copper–silica nano-LAMPs influenced by source chosen for refractive index profiles. Dispersion profiles for real (**a**) and imaginary parts (**b**) of refractive index. Extinction efficiencies using these profiles for 4-layered LAMP (**c**) with radii: {30, 35, 45, 50 nm} and 6-layered LAMP (**d**) with radii: {10, 15, 30, 35, 45, 50 nm}

efficiencies obtained using calculations with refractive indices obtained from Palik are much smaller especially in case of 6-layered LAMPs. Also, the resonances are shifted toward right to about $\sim$25 nm in case of both 4-layered and 6-layered LAMPs. The shifts in profiles in these cases are also in direct agreement with shifts in the absorption index. But in the case of silver–silica LAMPs, considerable differences exist in case of real part of refractive index as well leading to higher differences in the overall extinction. Hence, for broadband illumination applications, greater care is probably required in the fabrication and estimation of performance.

We have also made similar calculations of extinction for 4-layered and 6-layered copper–silica LAMPs and present them along with the refractive index profiles for copper from two sources in Fig. 4. The plasmonic resonances of copper are smaller in comparison with gold and silver in the illumination band and for the sizes considered here. But it can be clearly observed that the slight change in absorption index values indicating a slight shift toward longer wavelengths in the absorption index directly results in a shift toward longer wavelengths in resonance peaks.

As expected, results demonstrate that non-specificity in the choice of refractive index values when validating the LAMP structures could result in variability between theoretically predicted and experimentally obtained far-field characteristics. Typically, the refractive indices can be calculated by fitting experimental values with theoretical predictions from nanoparticles. But the variability in size and shape within metal nanoparticles (and/or LAMPs) could result in variability in the obtained refractive index profiles. To make accurate predictions, a range of refractive index values at each wavelength that could theoretically fit the extinction value based on the range of sizes for nanoparticles can be obtained. Such variability could also lead to pronounced effects also in case of internal hot spots generated depending on the sizes of layers. For example, Fig. 5 shows the internal electromagnetic field distribution in a 6-layered silver–silica LAMP at 785-nm excitation. Since Raman enhancement scales as fourth power of the local field obtained, we show local fields raised to power 4 here. The calculations made using refractive index from both sources differ, and the highest Raman enhancement obtained could differ up to two orders of magnitude in the outer silica shell.

The differences in hot spots generated could lead to significant lowering of the overall response of the LAMP, and the hot spot generated in and around it. In case of refractive indices from Johnson et al. [36], the real part of refractive index is lower and absorption index is higher at 785 nm. In this case, the absorption from the outer metal shells is greater resulting in higher energy reaching the internal metal surfaces which in turn is scattered. The absorbed radiation from outside shells and scattered radiation results in stronger plasmonic coupling and generation of hot spots of higher intensity and extent both internally and externally. An understanding of such variability can thus play a crucial role in engineering a probe structure for desired hot spots and validating it. It must be noted that the LAMP geometry in these situations provides more flexibility than simple structures such as nanoshells. The layer spacings and dielectric properties provide additional parameters that can be optimized to provide properties closer to desired.

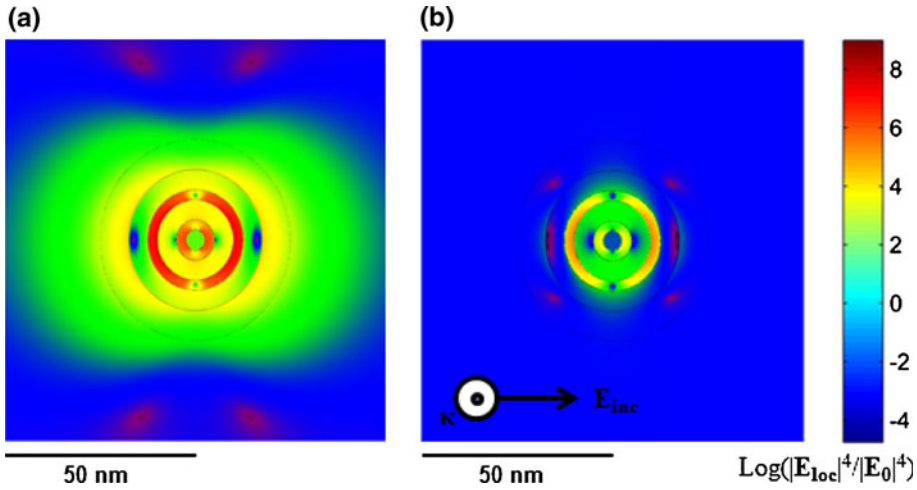

Fig. 5 Internal field distribution when illuminated by 785 nm plane wave in a 6-layered silver–silica LAMP: {5, 10, 20, 25, 35, 50 nm} using refractive index profiles from Johnson et al. [36] (**a**) and Palik et al. [37] (**b**)

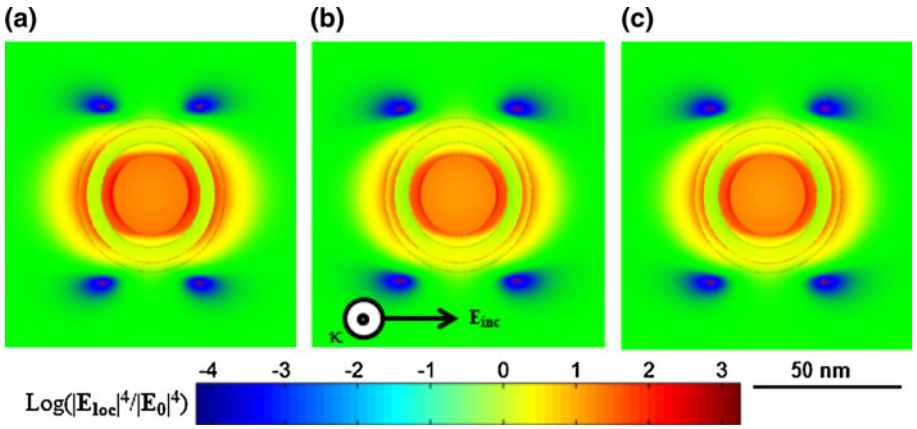

Fig. 6 Internal field distributions, when illuminated by 532 nm plane wave, for 4-layered gold–silica LAMP with radii {26, 34, 44, 50 nm} when considering **a** Silica refractive index dispersion, **b** silica and 1% rhodamine refractive index, and **c** silica and 10% Rhodamine refractive index

While we have considered the metal layer, the optical characteristics of LAMPs are also dependent on the dielectric properties of the silica shell. It is a common practice in the literature to use a dielectric constant of 2.04 [25] for fused silica. In the spectral regions being considered, however, silica has a slight dispersion profile. Also, the dye filled in silica shells could result in making the shell slightly absorptive. To investigate this effect, we have considered internal field distribution in a 4-layered gold–silica LAMP when illuminated by 532 nm plane wave (Fig. 6). The silica shells are considered to have a refractive index of 1.547 [46] and are filled with Rhodamine with a refractive index of $1.42 + 0.01i$ [47], and final refractive index has been calculated by using volumetric weightage. A comparison of calculations made for LAMPs with silica of refractive index 1.43 (Fig. 6a) as in previous cases with LAMPs with silica with its actual refractive index value linearly combined with having 1% Rhodamine (Fig. 6b) in it and 10% Rhodamine (Fig. 6c) in it is shown.

In the example considered here, the extent and intensity of hot spots generated have not changed significantly, but a slight change in the fields generated just outside the LAMP can be noticed. The dye considered here, Rhodamine, has molecular resonance only in the case of wavelength of excitation interest 532 nm, and hence, only this case is considered here. It is notable that the effect of changing the properties of the metal layers is significantly different from changing properties of the dielectric. Hence, fabrication efforts should be more concerned with maintaining the properties of metal layers. Efforts must also be expended to accurately measure and model the properties as a function of layer thickness and its crystal structure and volumetric properties (e.g. voids). The approach developed above can also improve our understanding of the differences between experimentally realizable values and theoretically predicted values for nanoLAMPs. When experimental measurement of nano-LAMPs are available, fitting their responses to parameters in the developed framework can provide exquisite knowledge of their structure and a measure of their variability in use.

3.2 Variation in shape

It is known that spheroidal particles of higher aspect ratio have the capability to generate narrower resonances and/or shift the resonance to longer wavelengths compared to

spherical particles. They can also generate higher intensity hot spots at the tips of the structures in the long axis. Use of non-spherical particles, however, presents a significant disadvantage in applications due to dependence of their optical response on the direction and polarization of the illuminating radiation. Spherical particles such as nano-LAMPs provide an opportunity for ease in fabrication as well as in elimination of any non-isotropic illumination.

During fabrication of nano-LAMPs, however, considerable variation in the spherical shape of the shells could result. Figure 7 shows the external field distribution of a Silica–Gold nanoshell evaluated through discrete-dipole approximation [48]. The refractive index value used for gold shell is taken from Johnson et al. [36], and 1.43 is used as refractive index for silica core. As the core is changed from spherical to prolate and then to oblate spheroidal core, the extent and the intensity of external hot spot generated is not effected to any significant level. This example demonstrates a simple variability in shape, and many other effects like bumps and craters as well as a Gaussian shape to the surfaces can be considered. These effects are likely to change the maximal local field generated, and the low concentration loading of the dye decreases the likelihood of dye being at such hot spots. Such examples do not represent the variability of shape for nano-LAMP. Further, considering multiple layers with different shapes will possibly effect the enhancement, but the above example shows that for small changes in shape, the hot spot will not vary in simpler cases. The general case in which multiple shells vary in different ways is, of

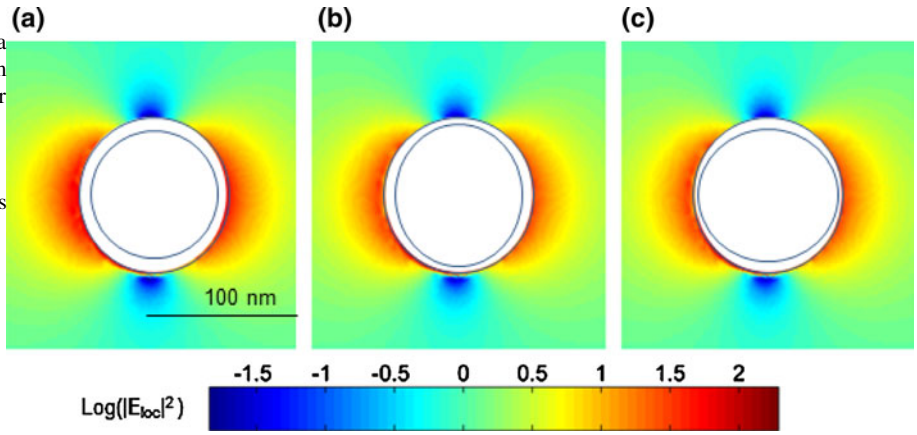

Fig. 7 External field distribution of gold–silica nanosphere {Gold core—40 nm, Silica shell—10 nm} when illuminated by 532 nm plane EM wave. Calculations are shown for **a** spherical core, **b** prolate spheroidal core (long axis diameter—45 nm, short axis diameter—40 nm}, and **c** oblate spheroidal core (long axis diameter—45 nm, short axis diameter—40 nm}. *Outer shell* surface is kept spherical and of constant size

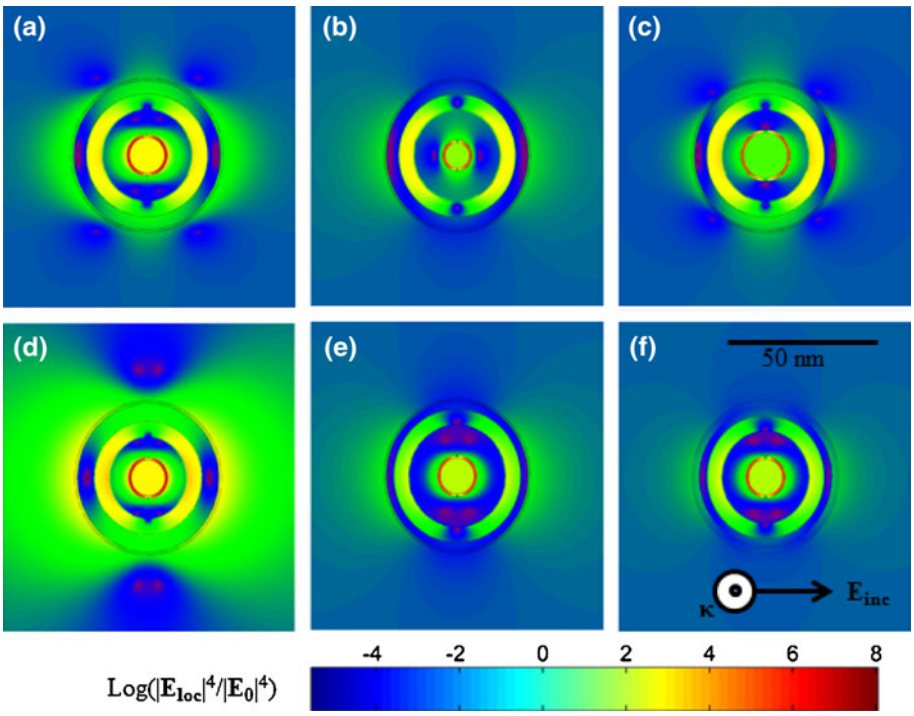

Fig. 8 Effect on local field distribution with slight variation in sizes of metal layers of gold–silica nano-LAMPs. **a** {7, 8, 16, 22, 29, 30 nm}, **b** {5, 6, 18, 24, 29, 30 nm}, **c** {9, 10, 18, 24, 29, 30 nm}, **d** {7, 8, 16, 22, 29, 30 nm}, **e** {7, 8, 20, 26, 29, 30 nm}, **f** {7, 8, 18, 24, 27, 30 nm}

course, difficult to predict due to the coupling of resonances between layers. Nevertheless, the simulation indicates that small variations in shapes of the inner layers are not likely to have a dramatic effect on the performance of the nano-LAMP.

3.3 Variation in size

A significant effect can be noticed by considering the size-induced changes in refractive indices of metals. Since this effect has already been discussed [38], we implement the proposed correction [26] and focus on variability in sizes obtained in the fabricated structures. The contributions from different metal shells in the overall response and plasmonic coupling can vary with small changes in the sizes of the layers. Also, nano-LAMPs are predominantly engineered by varying the layer sizes within for a desired hot spot or response. But the experimentally realized structures could possess slightly differing layer sizes due to variations in experimental conditions. Figure 8 shows the internal field distributions of a 6-layered gold–silica LAMP when illuminated by a 532 nm plane EM wave. Standard refractive index of 1.43 for silica and bulk values from Johnson et al. have been used for refractive indices of gold. The calculations are shown for reference structure in Fig. 8a, and slight changes to the size of metal core and outer metal layers have been made in the other sections. The intensity and extent of hot spots generated in each case are similar to those of reference, and since the dielectric spacing is kept constant, the volumetric summing of enhancement for the dye molecules is expected to remain the same. This example demonstrates that the slight variation in sizes of the metal shells does not result in any significant variation in the hot spot and hence the overall response for the LAMP structures for a given wavelength of excitation.

4 Conclusions

nano-LAMPs are multilayered metal-dielectric spheres that can produce greatly amplified responses for scattering- and absorption-based analytical techniques. The properties of nano-LAMPs are primarily dependent on the sizes of individual layers and dielectric properties of these layers. Since the resonances for which these structures are designed are very high and greatly non-linear, small variations from the designed parameters can result in variability of overall response. We have examined the effect of variability on LAMP signals due to the non-specificity of dielectric properties, size of the layers, and slight variation in the shape. The simulation results predict that structures with exceptional optical enhancements, for example, Raman enhancements up to eight orders of magnitude, can be designed. The variation in dielectric properties of the metal and silica layers, however, is shown to be crucial and can result in prediction differences up to two orders of magnitude in this signal. Differences in dielectric properties, further, can result in predicted far-field resonance peaks to shift up to 30 nm. These effects are dominant in silver, which has stronger plasmonic resonance characteristics, compared to those predicted for gold- and copper-based LAMPs. Slight changes in size and shape do not significantly affect the magnitude of the optical responses. Finally, it is predicted that LAMP structures can be designed to eliminate the effect of any variability due to small changes in size and shape. While the results provide confidence that small deviations in structure from ideal geometries will not preclude the use of LAMPS, experimental verifications of the predictions will be interesting in understanding both properties of materials at this scale as well as for designing probes for enhanced biochemical sensing.

Acknowledgments The study reported in this manuscript is supported in part by the National Science Foundation under Grant No. CHE 0957849 and the Beckman Institute's Seeding New Research Frontiers Program.

References

1. Faraday M (1857) Phil Trans of Royal Soc Lond 147:145–181
2. Prasad PN (2004) Nanophotonics. Wiley, London
3. Kawata S (2001) Near-field optics and surface plasmon polaritons. Springer, Berlin
4. Van Dijk MA, Tchebotareva AL, Orrit M, Lippitz M, Berciaud S, Lasne D, Cognet L, Lounis B (2006) Phys Chem Phys 8:3486–3495
5. Kelly KL, Coronado E, Zhao LL, Schatz GC (2003) J Phys Chem B 107:668–677
6. Eustis S, El-Sayed MA (2005) Chem Soc Rev 35:209–217
7. Noguez C (2007) J Phys Chem C 111:3806–3819
8. Camden JP, Dieringer JA, Wang Y, Masiello DJ, Marks LD, Schatz GC, Van Duyne RP (2008) J Am Chem Soc 130:12616–12617
9. Jain PK, Huang X, El-Sayed IH, El-Sayed MA (2008) Acc Chem Res 41:1578–1586
10. Chan GH, Zhao J, Hicks EM, Schatz GC, Van Duyne RP (2007) Nano Lett 7:1947–1952
11. Doering WE, Piotti ME (2007) Adv Mater 19:3100–3108
12. Kneipp J, Kneipp H, Kneipp K (2008) Chem Soc Rev 37:1052–1060
13. Oldenburg SJ, Averitt RD, Westcott SL, Halas NJ (1998) Chem Phys Lett 288:243–247
14. Xu H (2005) Phys Rev B 72:0734051–0734054
15. Chen K, Liu Y, Ameer G, Backman V (2005) J Biomed Opt 10:024005-1-6
16. Jackson JB, Westcott SL, Hirsch LR, West JL, Halas NJ (2003) Appl Phys Lett 82:257–259
17. Kodali AK, Bhargava R (2008) Proc SPIE 7032:70320V-1-10
18. Wustholz KL, Henry A-I, McMohan M, Freeman RG, Valley N, Piotti ME, Natan MJ, Schatz GC, Van Duyne RP (2010) J Am Chem Soc 132:10903–10910

19. Bukasov R, Shumkaer-Parry JS (2007) Nano Lett 7:1113–1118
20. Kodali AK, Llora X, Bhargava R (2010) Proc Natl Acad Sci 107:13620–13625
21. Li JF, Huang YF, Ding Y, Yuang ZL, Li SB, Zhou XS, Fan FR, Zhang W, Zhou ZY, Wu DY, Ren B, Wang ZL, Tian ZQ (2010) Nat Lett 464:392–395
22. Su X, Zhang J, Sun L, Koo T-W, Chan S, Sundararajan N, Yamakawa M, Berlin AA (2005) Nano Lett 5:49–54
23. Kodali AK, Bhargava R (2010) Chapter 15, Oxford Handbook of Science and Technology. Oxford University Press, Oxford
24. Averitt RD, Westcott SL, Halas NJ (1999) J Opt Soc Am A 16:1824–1832
25. Hu Y, Fleming RC, Drezek RA (2008) Opt Exp 16:19579–19591
26. Kodali AK, Schulmerich MV, Palekar R, Llora X, Bhargava R (2010) Opt Exp 18:23302–23313
27. Radloff C, Halas NJ (2004) Nano Lett 4:1323–1327
28. Prodan E, Radloff C, Halas NJ, Nordlander P (2003) Science 302:419–422
29. Lim DK, Jeon K-S, Hwang J-H, Kim H, Kwon S, Suh YD, Nam J-M (2011) Nature Nanotech 6:452–460
30. Johnson BR (1996) Appl Opt 35:3286–3296
31. Oldenburg SJ, Averitt RD, Westcott S, Halas NJ (1998) Chem Phys Lett 288:243–248
32. See KH, Mullins ME, Mills OP, Heiden PA (2005) Nanotechnology 16:1950–1959
33. Caruso F, Spasova M, Salgueirino-Maceira V, Liz-Marzan LM (2001) Adv Mater 13:1090–1094
34. Liz-Marzan LM, Correa Duarte MA, Pastoriza-Santos I, Mulvaney P, Ung T, Giersig M, and Kotov NA (2001) Core-shell nanoparticles and assemblies there of, Chapter 5. In: Nalwa HS (ed) Handbook of Surfaces and Interfaces of Materials, vol 3, pp 189–237
35. Xia X, Liu Y, Backman V, Ameer GA (2006) Nanotechnology 17:5435
36. Johnson PB, Christy RW (1972) Phys Rev B 6:4370–4379
37. Palik ED (ed) (1991) Handbook of optical constants of solids. Academic Press, New York
38. Khlebtsov B, Khlebtsov N (2006) J Biomed Opt 11:044002
39. Hao E, Li S, Bailey RC, Zou S, Schatz GC, Hupp JT (2004) J Phys Chem B 108:1224–1229
40. Moskovits M (2005) J Raman Spec 36:485–496
41. Morton SM, Jensen L (2009) J Am Chem Soc 131:4090–4098
42. Schatz GC, Van Duyne RP (2006) Handbook of vibrational spectroscopy. Wiley, London
43. Mulvaney SP, Musick MD, Keating CD, Natan MJ (2003) Langmuir 19:4784–4790
44. Bohren CF, Huffman DR (1983) Absorption and scattering of light by small particles. Wiley, London
45. Wiscombe WJ (1980) Appl Opt 19:1505–1509
46. Ghosh G (1999) Optc Comm 163:95–102
47. Leupacher W, Penzkofer A (1984) Appl Opt 23:1554–1557
48. Draine BT, Flatau PJ (1994) J Opt Soc Am 4:1491–1499